

Friction damping and forced-response of vibrating structures: an insight into model validation

*Original*

Friction damping and forced-response of vibrating structures: an insight into model validation / Umer, M., Gastaldi, C., Botto, D.. - In: INTERNATIONAL JOURNAL OF SOLIDS AND STRUCTURES. - ISSN 0020-7683. - ELETTRONICO. - 202:(2020), pp. 521-531. [10.1016/j.ijsolstr.2020.07.002]

*Availability:*

This version is available at: 11583/2841296 since: 2020-07-24T09:25:46Z

*Publisher:*

Elsevier

*Published*

DOI:10.1016/j.ijsolstr.2020.07.002

*Terms of use:*

This article is made available under terms and conditions as specified in the corresponding bibliographic description in the repository

*Publisher copyright*

(Article begins on next page)

# Friction damping and forced-response of vibrating structures: an insight into model validation

Daniele Botto<sup>a,\*</sup>, Chiara Gastaldi<sup>a</sup>, Muhammad Umer<sup>b</sup>

<sup>a</sup>*Department of Mechanical and Aerospace Engineering - Politecnico di Torino, 10129  
Torino, Italy*

<sup>b</sup>*Mechanical Engineering Department - Institute of Space Technology, Islamabad,  
Pakistan*

---

## Abstract

Dry friction is widely incorporated in turbomachinery, in the form of under-platform dampers, to limit vibrations at resonance and reduce risks of high-cycle fatigue failures. Most of the test rigs that have been used to investigate the behavior of under-platform dampers aim at evaluating the damper performance in terms of reduction of forced-response amplitude in blades. This approach could be insufficient to understand local nonlinearities of the contact and the influence of dampers on blade dynamics. A newly developed test rig provides the authors with an unprecedented set of information. It is capable to measure contact forces and relative displacements between dampers and blade in addition to the overall blade dynamic response. This controlled environment, together with an effective model of the blade/dampers system, is used to provide an insight into the subject of model validation. The presented experimental and numerical study of the damper is used to highlight

---

\*Corresponding author

*Email addresses:* `muhammad.umer@ist.edu.pk` (Muhammad Umer),  
`chiara.gastaldi@polito.it` (Chiara Gastaldi), `daniele.botto@polito.it` (Daniele Botto)

*Preprint submitted to International Journal of Solids and Structures*

the relevance of an accurate representation of the constraints induced by friction contacts and to discuss the adequacy of state-of-the-art contact models.

*Keywords:*

Turbine blade vibrations Nonlinear dynamics Friction damping

Under-platform damper Test rig Contact force measurement

---

## 1. Introduction

Dry friction damping is used, in the field of turbomachinery, to mitigate the structural vibrations caused by fluctuating stresses [1, 2]. Under-platform dampers (UPDs) are small metallic components placed between two consecutive blades of a turbine to minimize the blade vibration by dissipating the energy at the contact interface. Highly nonlinear behavior of the frictional contacts makes it challenging for researchers and engineers to precisely model and predict the response of complete blade/damper system. In this regard, explicit numerical models of UPDs are used with a multi-harmonic balance solver to predict their non-linear behavior. A detailed study on the modelling of UPDs is presented by several authors [3–10] in which a suitable contact model is adopted to compute the damper contact forces as a function of given relative displacement between two contact surfaces. These contact models must be calibrated. This step is crucial as numerical results are strongly dependent on the chosen set of contact parameters namely friction coefficient and contact stiffness, [10–13]. Therefore, experimental measurements are necessary:

- to determine the performance of the damper in terms of blade amplitude reduction and frequency shift;

20     • to estimate the contact parameters used to calibrate contact models.

These two necessities are sometimes fulfilled with the same set of experimental evidence usually in the form of Frequency Response Functions (FRFs) [7, 14–16]. Unfortunately, model updating based on contact parameters to obtain the desired frequency response is not a viable practice, as multiple combinations of these parameters may produce the same frequency response giving an under-determined problem. Another way to obtain contact parameters is through the use of single-contact test arrangements[17–19]. A test rig improved in [20] is capable of measuring friction coefficients and contact stiffness values of a flat-on-flat contact interface. This test rig has a facility to control the relative displacement and high temperature of the contacting surfaces. However, the applied normal load is constant, which is not consistent with the real working conditions of UPDs. An upgrade first proposed in 2010 [21] has a single damper constrained between two dummy platforms. A feedback controlled displacement is provided with the help of piezoelectric actuator on one of the platform whereas, damper contact forces are measured on the other platform by using two load cells. Since then, this test rig has been used to investigate the kinematics of several dampers [22, 23]. As in this test rig the blade platform kinematics is imposed by the experimenter, the effect of damper on the blade dynamics is not present. Therefore, a novel test bench [24, 25] has been designed by the authors to overcome these limitations and to investigate the relationship between the damper kinematics and blade dynamics (a topic of recent interest in the community [10]). This experimental setup is composed of a single turbine blade with two UPDs and has a facility to measure the damper contact forces, its relative displacement

45 with respect to the blade and the blade response.

Data obtained with this experimental setup establish a base to study the behavior of dampers at their contact level. Moreover, the measured contact forces offer the unprecedented opportunity to validate directly the Finite Element (FE) model of the blade subjected to nonlinear contact forces. In fact, measured contact forces can be applied as external forces on the FE model of the blade. The resulting numerical FRF can then be compared to its experimental counterpart. Results of this comparison show that given combinations of blade mode shape and platform angles lead to very small contact forces, close to the accuracy of the measuring device. Uncertainty in the amplitude and phase of the contact forces could prevent the test rig from gathering meaningful evidence from the contact forces signal. Furthermore, very small contact forces can lead to a negligible effect of the damper on the blade dynamics. The purpose of the paper is to develop a procedure to evaluate the sensitivity of the contact forces to different platform angles. To this end the idea of implicit stiffness has been introduced. The authors believe that the proposed approach will provide guidance in the design of any laboratory set-up and in the estimation the UPD potential in realistic working conditions.

65

This paper is organized as follows: Sect. 2 gives a brief description of the test rig used in the experimental campaign; Sect. 3 addresses the numerical model of the blade while Sect. 4 shows the procedure used to validate the dynamic model in which the contact forces between under-platform and

70 damper are replaced by their measured counterparts; Sect. 5 presents and  
validates a numerical tool that, for a given blade model, maps the contact  
forces as a function of the platform angles; Sect. 6 summarizes the results  
and the main achievements of the paper.

## 2. Experimental Setup

75 The feature that best distinguishes the present test rig from others found  
in the literature is the direct measurement of the contact forces when the  
damper is dynamically coupled with the blade. A top view of the test rig  
is shown in Fig.1 which presents a single turbine blade and two dampers in  
contact with the under-platform of the blade on one side and with a ground  
80 platform on the other side. Each ground platform, one for each damper, is  
linked to a contact force measuring system. The two ground platform are  
referred to as “Even” or “Odd” after the serial number of the load cells in-  
stalled on that platform. A component named L-Separator, designed with  
two orthogonal limbs, separates the contact forces into two components act-  
85 ing along each limb axes. A piezoelectric load cell is placed at the end of  
each limb to measure the respective force component. A controllable and  
measurable pushing force  $F_P$  is applied on the root of the blade - to simulate  
the actual centrifugal force which acts on the blade while the turbine runs,  
see also Fig. 2 - through a pushing block. A complete description of the rig  
90 and of its force measuring system is given in [25].

The contact forces at the blade platform side are inferred from the mea-  
sured contact forces at the ground platform side through a simple force equi-

librium, depicted in Fig. 2. The damper inertia forces are here neglected, a  
95 perfectly valid assumption at frequencies lower than 5 kHz as demonstrated  
in [26]. Forces are decomposed into their normal (N) and tangential (T)  
components, as shown in Fig. 2, or along the blade axial-radial directions  
(XYZ reference system). This last reference system is the same used in the  
FE model of the blade and will be used throughout the paper. The blade  
100 excitation is provided by means of an electromagnetic shaker. The shaker  
stinger is connected at a point near the blade root (low mobility point) to  
excite the structure at a given frequency with the desired excitation level.

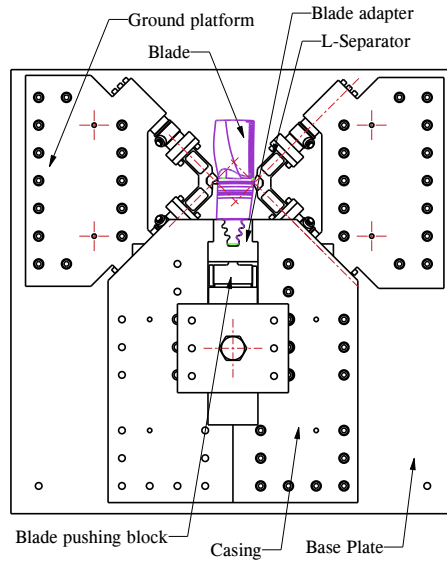


Figure 1: Top view of test rig

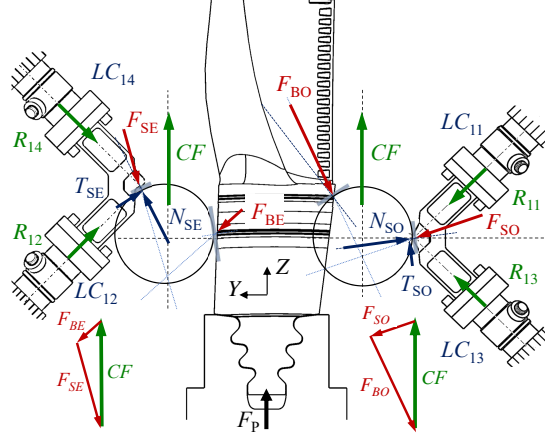


Figure 2: Damper static force equilibrium.  $R_{ij}$  are the forces read by load cells  $LC_{ij}$ . Contact forces are denoted to as  $F$  with  $N$  and  $T$  normal and tangential components respectively. Subscript  $S$  or  $B$  means force on Support or Blade, while  $E$  or  $O$  denotes the “Even” or the “Odd” side. Sides are named Even or Odd after the serial number of the load cells installed on that side. The static load  $CF$ , simulating the Centrifugal Force on dampers, is applied with dead weight.

### 3. The blade numerical model

The general dynamic equation of any friction-damped system can be written as

$$\mathbf{M}\ddot{\mathbf{Q}} + \mathbf{C}\dot{\mathbf{Q}} + \mathbf{K}\mathbf{Q} = \mathbf{F}_E + \mathbf{F}_C \quad (1)$$

where  $\mathbf{M}$ ,  $\mathbf{C}$  and  $\mathbf{K}$  correspond to mass, damping and stiffness matrices of the system respectively. In Eq.1, vector  $\mathbf{Q}$  represents the displacement of all degrees of freedoms (DOFs) of the system. Vectors  $\mathbf{F}_E$  and  $\mathbf{F}_C$  correspond to external and contact forces respectively. In the present case, the external force  $\mathbf{F}_E$  was applied by using an electromagnetic shaker, whereas  $\mathbf{F}_C$  are nonlinear forces at the blade platform-damper contact interface. The mass

110 and stiffness matrices of the blade were obtained using a commercial FE code. The number of DOFs in a FE model is generally very high, so it could be very demanding to run dynamic analysis if non linearity due to contact problems are present. Moreover, commercial codes are not so flexible and open-source to accept external routines developed by users to solve special  
115 problems or to test new solution methods. For these reasons the mass and stiffness matrices of the full FE model were reduced and exported to be used together with in-house developed codes.

### *3.1. Craig-Bampton Model Order Reduction*

The Craig-Bampton reduction method, also known as CB-CMS, is a com-  
120 monly used technique to reduce the size of a large FE model by acquiring the fundamental frequency modes of the structure [27, 28]. In this method, only a subset of physical DOFs of the full model, corresponding to chosen nodes, are retained as master DOFs while the remaining DOFs are reduced in a set of orthogonal modes (slave DOFs). In the blade FE model presented in this  
125 paper and shown in Fig. 3, master nodes include contact nodes at the blade platforms and at the root attachment, one blade excitation node where the shaker is attached and a blade response node where the accelerometer is positioned. It was here chosen to apply the CB-CMS technique to the free blade model. Matrices  $\mathbf{M}$  and  $\mathbf{K}$  thus become  $\mathbf{M}_{\mathbf{R}}$  and  $\mathbf{K}_{\mathbf{R},\text{free}}$ . The structure will  
130 be constrained to reproduce the clamping of the root, at a subsequent step. Section 3.3 gives further details on this matter.

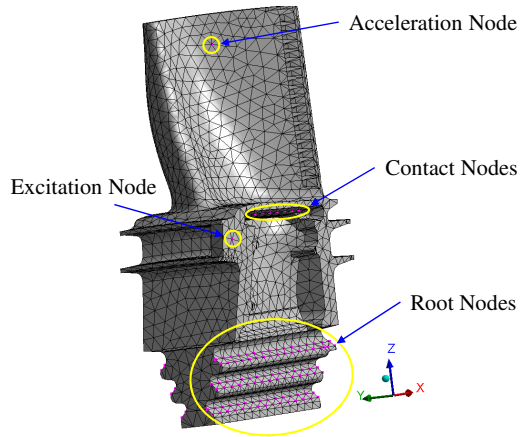


Figure 3: Finite element model of the blade and selected master nodes for CB-CMS reduction. Master nodes on one platform and one side of the root are hidden because of the orientation of the blade.

### 3.2. Blade Model Updating

The FE model of the blade was updated to match the first two measured natural frequencies (see response depicted in Fig. 4) in free-free conditions, i.e. without damper and blade root constraints. The Young modulus was chosen as the updating parameter while the density was estimated by measuring the blade weight with a high precision scale and assuming a uniform distribution of the mass on the 3D model. It was found that with a Young's modulus of 210,000 MPa the first two resonances of the free-free blade (5652.7 and 7567.3 Hz) match well with the measured values (5652.5 and 7557.5 Hz).

### 3.3. Applying clamp boundary conditions

A very high clamping force  $F_P$  of 150 kN was applied on the blade. This high clamping force minimizes the relative displacement between the blade

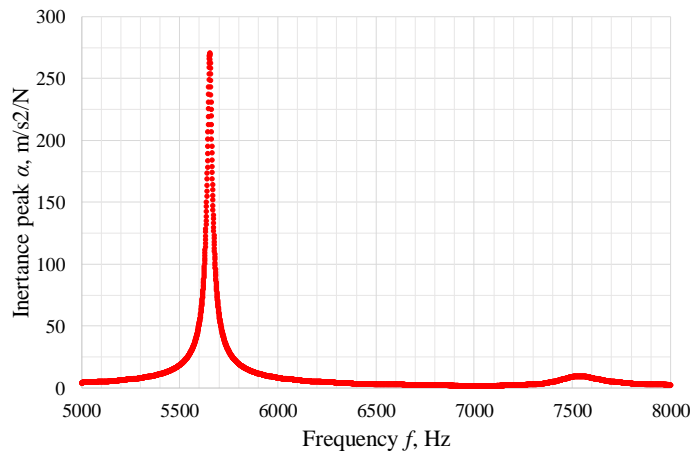


Figure 4: Measured FRFs of free-free blade.

root and its slot and thus the resulting damping at the root becomes negligible. The blade clamping was modeled by introducing a 3D spring element at each node on the blade roots, as shown in Fig.5. The 3D spring element may connect each selected blade root node either to a corresponding node on the surrounding structure (if the disk is modeled) or simply to ground (if, as in this case, the bulkiness and stiffness of the blade adapter allows for this simplification.)

The use of a 3D spring element (which may be easily upgraded to an actual contact element capable of slip if deemed necessary) allows modeling the effect of compliance of the contact interface in all directions. The 3D spring element needs two calibration parameters:  $k_n$  and  $k_t$ , i.e. it is here assumed that the tangential stiffness in the two uncoupled directions shown in Fig. 5. share the same value  $k_{t1} = k_{t2} = k_t$ . The values of the stiffness were determined by imposing that the first two measured frequencies  $f_{meas}$  of the

clamped-free (i.e. no damper) blade match the simulated ones  $f_{sim}$ ,

$$\begin{cases} f_{1,meas} = f_{1,sim}(k_n, k_t) \\ f_{2,meas} = f_{2,sim}(k_n, k_t) \end{cases} \quad (2)$$

Matrix  $\mathbf{K}_{\mathbf{R},free}$  from Sect. 3.1, is thus substituted by matrix  $\mathbf{K}_{\mathbf{R}}$ .

The damping contribution of the blade root is not accounted by the springs  
 145 (as no microslip is allowed at this stage). The (minor) contribution to damp-  
 ing given by the blade root together with the structural (material) damping  
 of the blade is accounted through matrix  $\mathbf{C}_{\mathbf{R}}$ . The modal damping was esti-  
 mated using the measured FRFs of the clamped free (i.e. no damper) blade  
 as a reference. The damping ratios  $\zeta$  were found to be 0.032 and 0.022 for the  
 150 first and the second mode respectively; the resulting experimental-numerical  
 comparison is shown in Fig. 6.

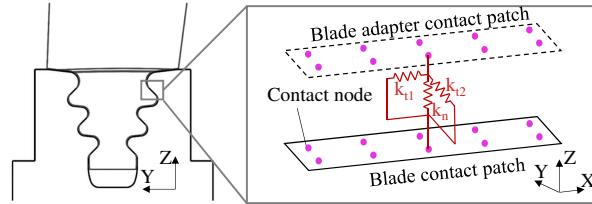


Figure 5: 3D spring compliance introduced to simulate the blade root constraints.

### 3.3.1. Forced response calculation

This section gives further details on the method used to solve system of Eq. 1. Harmonic balance is used to compute the steady state solution of these equations where an applied periodical excitation force of frequency  $\omega$  results in the periodical response of the system [29, 30]. If the damper is not present (i.e. clamped-free blade), then  $CF = 0$ , the equilibrium is linear

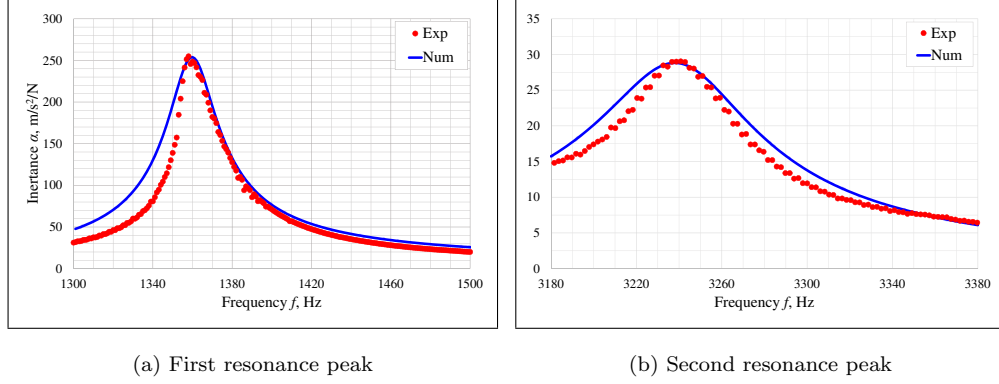


Figure 6: Comparison between measured and simulated FRFs of the blade after the contact stiffness and the damping in the numerical model has been updated to an optimal value.

and can be solved, in the frequency domain, as a simple system of algebraic equations

$$\bar{\mathbf{Q}}^1 = (-\omega^2 \cdot \mathbf{M}_{\mathbf{R}} + i \cdot \mathbf{C}_{\mathbf{R}} + \mathbf{K}_{\mathbf{R}})^{-1} \bar{\mathbf{F}}_{\mathbf{E}}^1 \quad (3)$$

where matrices  $\mathbf{M}$  and  $\mathbf{K}$  have been substituted with their CB-CMS reduced counterpart, later constrained at the root  $\mathbf{M}_{\mathbf{R}}$  and  $\mathbf{K}_{\mathbf{R}}$  and  $\bar{\mathbf{Q}}^1$  and  $\bar{\mathbf{F}}_{\mathbf{E}}^1$  represent the first harmonic Fourier components of the displacement and external force vectors respectively. Equation 3 can be written in a short form as

$$\bar{\mathbf{Q}}^1 = \mathbf{D}(\omega)^{-1} (\bar{\mathbf{F}}_{\mathbf{E}}^1), \quad (4)$$

whereas  $\mathbf{D}(\omega)$  corresponds to the dynamic stiffness matrix  $\mathbf{D}(\omega) = (-\omega^2 \mathbf{M}_{\mathbf{R}} + i \mathbf{C}_{\mathbf{R}} + \mathbf{K}_{\mathbf{R}})$ . If, on the other hand, the damper is present, contact forces  $\mathbf{F}_{\mathbf{C}}(\mathbf{Q}, \dot{\mathbf{Q}})$  are non-zero. These forces are due to Coulomb friction nonlinearities and are typically determined as a function of relative displacements at the contact using a suitable contact model [31]. Given the dependence of contact forces on displacements, the equations are clearly nonlinear. As a re-

sult, iterative techniques such as Newton-Raphson or Continuation methods are applied [32].

In the present paper the theoretical contact forces has been replaced by the directly measured contact forces. Both measured contact forces and external forces are transformed in the frequency domain using fast Fourier transform (FFT), and applied to the clamped-free blade model so that Eq. 4 becomes

$$\bar{\mathbf{Q}}^1 = \mathbf{D}(\omega)^{-1} \left( \bar{\mathbf{F}}_{\mathbf{E},\text{meas}}^1 + \bar{\mathbf{F}}_{\mathbf{C},\text{meas}}^1 \right). \quad (5)$$

The dependence of contact forces on relative displacements is still present, in fact different experimental conditions (different  $\omega$ , different excitation levels  $|\mathbf{F}_{\mathbf{E}}|$ ) yield different measured values of  $\mathbf{F}_{\mathbf{C}}$ . However, no assumption on the  
 155 formulation of this displacement-contact force relation is needed at this stage. The authors are willingly separating the validation of the blade dynamic model (results in Sect. 4) from the assessment of the adequacy of the contact model formulation.

#### 160 4. Validation of the dynamic model blade with virtual constraints

The objective of this section is to verify if the forced response computed using the clamped FE model of the blade, fed with the measured contact forces values, is capable to replicate the measured FRF. The blade response was simulated applying the procedure explained in Sect. 3. The steps of the  
 165 validation procedure are summarized below and displayed graphically in Fig. 7.

1. The blade was excited with a sinusoidal force, applied through a shaker, whose amplitude was set at  $|\mathbf{F}_{\mathbf{E}}| = 1$  N in all studied cases.

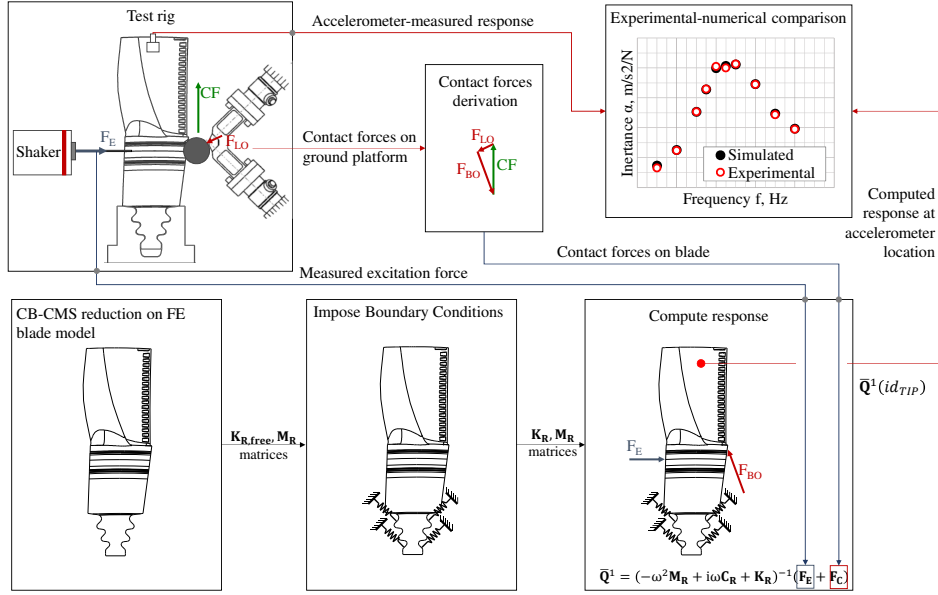


Figure 7: Algorithm describing the validation of the linear blade dynamic model

2. Contact forces were measured at the ground platforms side of both dampers, whereas force components applied on the blade were inferred through the damper static force equilibrium (Fig. 2).
3. Response of the blade, in terms of inertance, was recorded by an accelerometer located at the tip of the blade.
4. The full FE model of the blade was reduced with the CB-CMS method, see Sect. 3.1, yielding to the a set of stiffness and mass matrices  $\mathbf{K}_{\mathbf{R},\text{free}}$  and  $\mathbf{M}_{\mathbf{R}}$ .
5. A set of contact springs was applied to the root contacts as described in Sect. 3.3. The reduced order stiffness matrix  $\mathbf{K}_{\mathbf{R},\text{free}}$  thus becomes  $\mathbf{K}_{\mathbf{R}}$ .
6. The first harmonic of both the excitation and contact forces were mimicked in the numerical environment according to Eq. 5.

7. Experimental and simulated inertance were compared.

The uncertainty level of contact force measurements is in the  $[0.50\div 0.75]$  N range, and cannot be reduced further due to mechanical tolerances, electronics, signal/noise ratio and uncertainty involved in the estimation of platform angles. Details on contact forces calculation and quantification of their uncertainty can be found in [25]. It will be shown that, depending on the magnitude of harmonic variation of the contact forces, the uncertainty level of the forces may hinder the validation procedure.

#### 190 *4.1. Noise effect on measured contact forces*

As a first trail, both dampers were assembled at their nominal position with respect to blade as shown in Fig. 2. A number of experiments were performed, under the same nominal experimental conditions, to measure the contact forces on both sides and the blade response. Figure 8 shows two examples of simulated responses compared with their measured counterpart. A slight variability can be detected in the measured responses despite the same nominal conditions of the test. This variability is not surprising as the dampers contact conditions may be different even if the external loads on blade and dampers are nominally the same [24, 25]. More concerning, is the poor repeatability (only two examples are reported but this effect is present in all the tests performed) and the huge discrepancy with respect to the measured response which would make the proposed method completely unreliable. After carefully checking the numerical procedure the authors concluded that the cause of this disagreement did not reside in the model itself, rather in the measured contact force signals fed to the model.

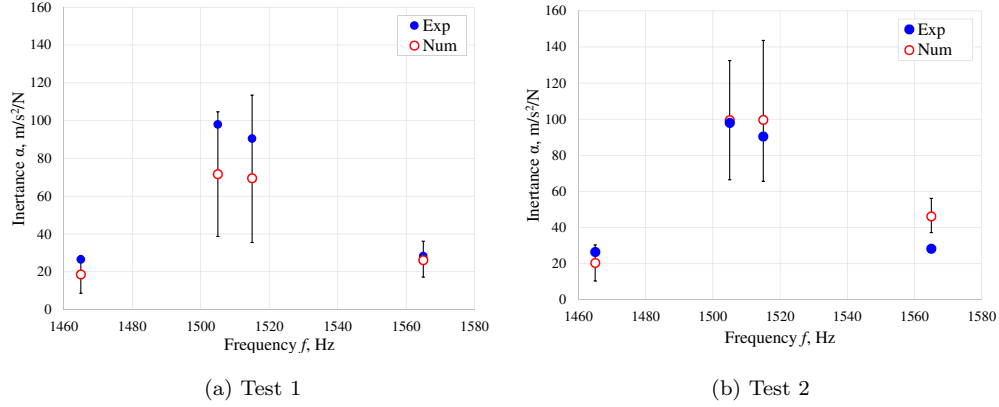


Figure 8: Comparison between numerical and experimental results of blade response amplitude for the same nominal loading conditions  $CF=26$  N and  $\mathbf{F}_E=1$  N.

To identify the source of errors two simpler experimental configurations were investigated. In each test setup only one damper at a time was installed on one side of the blade, as depicted in Fig. 9. The numerical-experimental comparison of both cases is shown in Fig. 10. Still a large discrepancy between the measured FRF and the numerical “prediction” can be observed in the first case when only the even side damper is active, Fig. 10a. Whereas, in the case in which the odd side damper is active, numerical results perfectly match with the experimentally measured amplitude response of the blade, as shown in Fig. 10b.

#### 4.2. Unsuccessful numerical-experimental comparison

The contact forces are composed of two parts: the “static” component that balance the simulated centrifugal force  $CF$  on the damper and the “dynamic” component (also referred to as “harmonic” component) deriving from the blade movement. Figure 11 shows the contact forces on the even and odd side platforms. In this figure, the contact forces are sketched at two distinct

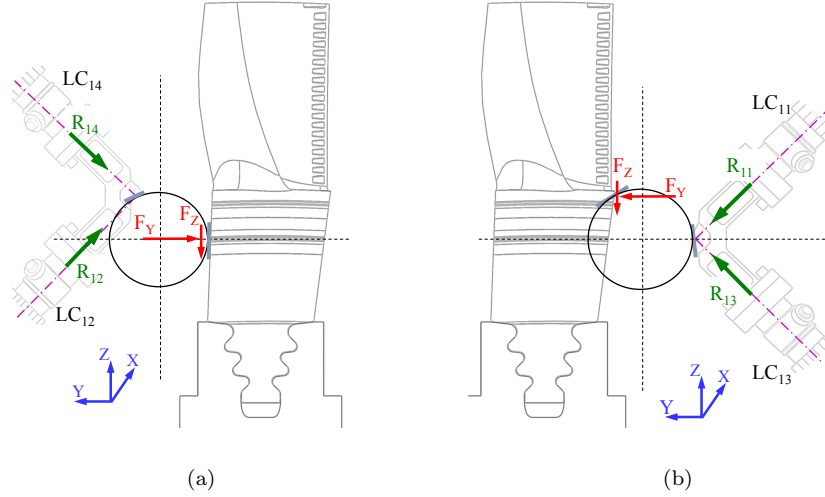


Figure 9: (a) Even side damper placed at its nominal position to measure contact forces.  
 (b) Odd side damper placed at its nominal position to measure contact forces

time points during blade movement - denoted by superscript prime and double prime - to emphasize the change, in magnitude and inclination, induced by blade dynamics. By carefully observing the contact forces on the even side platform, Fig. 11a, it is clear that the variation of force ranges between 1 to 2 N at the most. The magnitude of the harmonic variation of the force depends upon the contact angles and the platform kinematics (i.e. experimental set-up and blade mode shape). The level of uncertainty on the contact force,  $\approx 0.75$  N according to the sensitivity analysis performed in [25], is almost 50% of the force magnitude. This observation can easily explain the very large discrepancies between the numerical and experimental results: the platform blade has been loaded with a measured force whose measurement accuracy is of the same order of magnitude as the force itself.

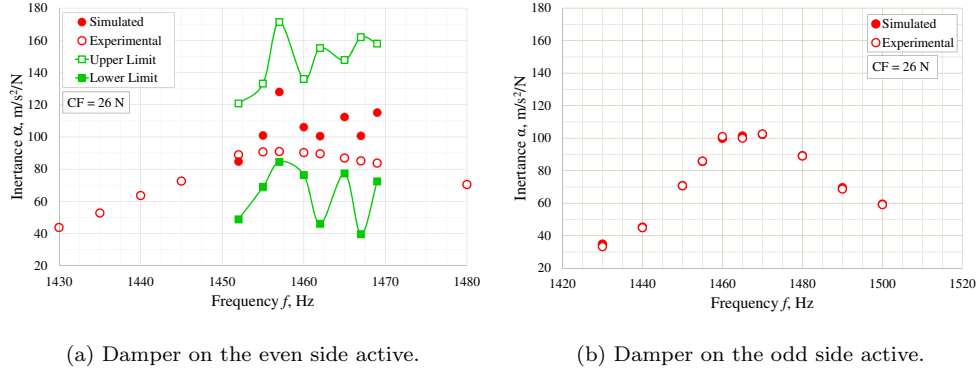


Figure 10: (a) Error sensitivity of blade response amplitude due to even side contact forces measurement at  $CF = 26$  N. (b) Numerical vs Experimental results comparison for damper forces measured on Odd side at  $CF = 26$  N

235 A sensitivity analysis was carried out to further evaluate the effect of the contact force measurement accuracy on the blade response. A sinusoidal perturbation was added to the contact force with a post-processing treatment of the measured signals. The amplitude of this perturbation was equal to the maximum level of uncertainty (0.75 N) with a phase shift that ranged from

240 0 to 15 degrees with respect to the measured contact force. The upper and lower bound of the blade response produced by the perturbed contact force are shown in Fig. 10a. It is evident that even a seemingly small perturbation of this force can have a significant impact on the blade amplitude response.

#### 4.3. Successful numerical-experimental comparison

245 The second validation attempt was tested with only the even side damper activated, according to the configuration shown in Fig. 9b. The different contact angles of this configuration and the consequent platform kinematics, if compared with the results obtained with the activation of only the even

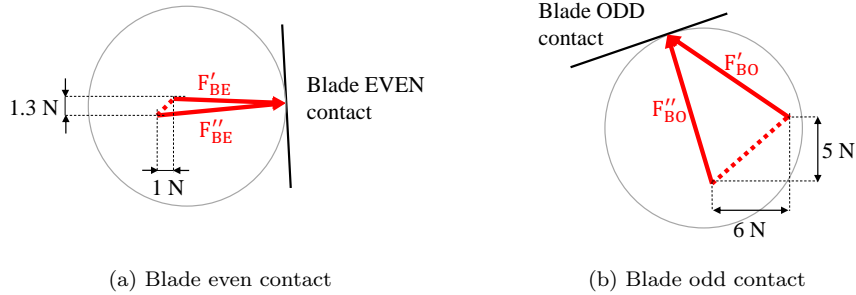


Figure 11: Measured contact force on the blade platform on the even and odd side,  $\mathbf{F}_{BE}$  and  $\mathbf{F}_{BO}$  respectively. The two forces on each side,  $\mathbf{F}'_{B}$  and  $\mathbf{F}''_{B}$ , are represented at two distinct time points of the same analysis. The picture emphasizes the variation of the contact forces caused by the blade movement.

side damper, produces

- 250 • higher harmonic variation of the measured contact forces that in this case range between 5 and 8 N, as shown in Fig. 11b;
- a stiffening effect, for which the peak in Fig.10b is now sharper and few Hz higher than that shown in Fig. 10a.

Furthermore, in this case, the uncertainty level guaranteed by the load  
 255 cell measurement is adequate and reasonably smaller than the force signals themselves. As a result, the validation procedure summarized in Eq. 5 can be safely applied. Experiment were performed for three levels of load  $CF$  on the damper, namely 26, 46 and 86 N. Comparison between numerical ad experimental results are shown in Fig. 10a ( $CF = 26$  N) and Fig. 12 ( $CF$   
 260 = 46 and 8): numerical results match their experimental counterpart quite satisfactorily in all investigated cases.

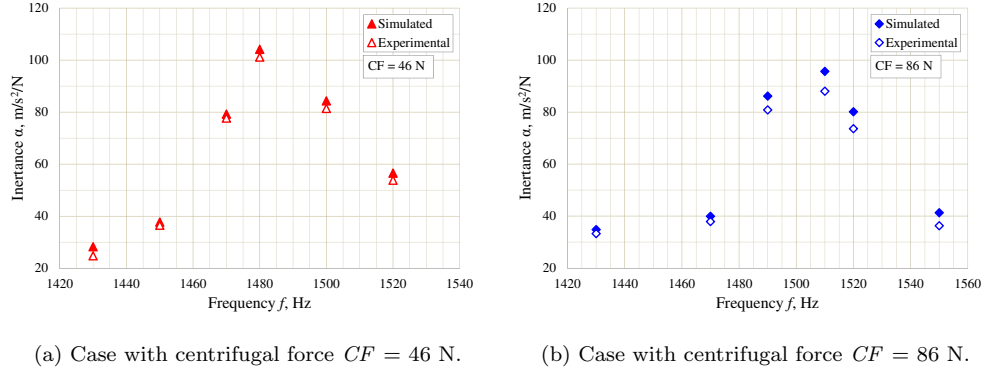


Figure 12: Comparison of numerical and experimental frequency response amplitude for different loads  $CF$  on the damper.

## 5. Predicting influence of platform angles on the contact forces magnitude

Section 4 has shown that, depending on the damper position (i.e. the contact angles), the resulting amplitude of the harmonic component of the contact forces may change significantly. Attaining harmonic contact forces of adequate amplitude on the blade is of paramount importance, both in the laboratory environment and in real working conditions. An insufficient harmonic contact force amplitude influences the quality of the measurement in the lab as shown in Sect. 3, while it may impair the damping and stiffening effectiveness of the UPD as demonstrated in [33].

The purpose of this section is to provide the experimenter and blade/damper designer with a tool to predict the magnitude of the contact forces for different sets of platform angles.

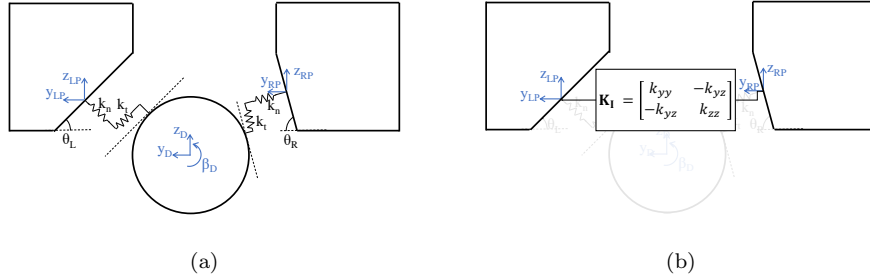


Figure 13: (a) 2D view of a damper between neighboring platforms in full stick condition. (b) Equivalent implicit stiffness concept.

275 *5.1. The implicit stiffness concept*

As shown in [34], the cylindrical damper analyzed in this paper never leaves the microslip condition. Therefore a conservative and representative modeling choice sees the damper in full stick (i.e. linked to the surrounding platforms by means of simple contact springs), as shown in Fig. 13a.

280 Since the damper is modeled as a rigid body and the position of the contact points is known (i.e. determined by the contact angles  $\theta_L$  and  $\theta_R$ ), it is convenient to substitute the presence of the damper with a set of equivalent springs, here termed implicit stiffness matrix  $\mathbf{K}_I$  and represented in Fig. 13b. This substitution willingly neglects the mass and inertia contribution of the damper: this simplification is allowed since, as demonstrated in  
 285 [35], the damper inertial effects become significant only for frequencies  $>50$  kHz. In other words, the implicit stiffness  $\mathbf{K}_I$  takes into account the value and the position of the contact springs: the entries of matrix  $\mathbf{K}_I$  are linear combinations of the normal and tangential contact stiffness  $k_n$  and  $k_t$ , whose  
 290 specific values have been determined according to [34]. The reader can refer to Appendix A for the complete derivation of  $\mathbf{K}_I$ .

### 5.2. A step-by-step procedure

This section aims at providing the reader with a series of instructions to predict the influence of the platform angles on the amplitude of the harmonic component of the contact forces. This task is of primary importance as it has been shown in Sect. 4 that the amplitude of the harmonic component of the contact forces can impair the .

This procedure can be considered a standard sensitivity analysis. The input parameter space is composed by the two variables  $\theta_L$  and  $\theta_R$  which are explored in the  $[0 - 90]^\circ$  range. The "input" data of the sensitivity analysis is the FE model of the structure of interest. The following procedure, visualized in Fig. 14, is repeated for all possible combinations of variables  $\theta_L$  and  $\theta_R$  explored in the range of interest.

3. The user adds the implicit stiffness contribution  $\mathbf{K}_I(\theta_L, \theta_R)$ , therefore matrix  $\mathbf{K}_R$  turns into matrix  $\mathbf{K}_{R,stick}$ . In the present case the user is trying to replicate the test condition from Fig.9, therefore  $\mathbf{K}_I$  is placed between contact nodes belonging to one of the platforms (either even or odd side) and the ground<sup>1</sup>.

---

<sup>1</sup>This procedure is taking advantage of two simplifications outlined below.

- (a) The ground platform is here not modeled since, as shown in [25], its stiffness is at least one order of magnitude larger than that of the blade and of the contact  $k_n$  and  $k_t$ .
- (b) In principle the blade platform geometry (i.e. inclination) should be updated to accommodate the different  $(\theta_L, \theta_R)$  combinations. However this minor geometrical change will not affect the subsequent eigenvalue analysis, therefore this step can be safely neglected.

4. Perform an eigenvalue analysis on matrices  $\mathbf{K}_{\mathbf{R},\text{stick}}$  and  $\mathbf{M}_{\mathbf{R}}$  and isolate  
310 the mode of interest, here termed  $\phi_n$ .
5. The entries of mode  $\phi_n$  corresponding to the platform contact nodes  
DOFs represent the platform motion trajectory  $\phi_n(id_C)$ .
6. The normalized platform motion trajectory  $\frac{\phi_n(id_C)}{|\phi_n(id_C)|}$  multiplied by the  
implicit stiffness matrix  $\mathbf{K}_{\mathbf{I}}$  yields the vector of normalized contact  
315 forces  $\mathbf{f} = (f_y, f_z)'$ .

The procedure is repeated for all  $(\theta_L, \theta_R)$  of interest. The  $y$  and  $z$  components of the target vector  $\mathbf{f}(\theta_L, \theta_R)$  can then be plotted as a function of the two variables  $(\theta_L, \theta_R)$ . The results for a blade-single damper configuration (similar to those shown in Fig. 9) can be found in Fig. 15. In detail, the  
320 results related to the set-up which sees the damper on the left (even) side of the blade can be found in Fig. 15a, those related to the damper on the right (odd) side in Fig. 15b.

### 5.3. Results discussion

For each configuration, one point on the  $(\theta_L, \theta_R)$  plane corresponds to  
325 the specific blade tested by the authors. This point has been highlighted in Fig. 15. The comparison between the even and odd configuration fully confirms the experimental results discussed in Fig. 11: the response surface related to the even side configuration has a minimum in the area where the experimental point lies. It is worth noting that, had this tool been available  
330 to the authors before the start of the experimental campaign, the even side configuration would have been immediately discarded, thus saving time and effort.

This comparison confirms the goodness of the implicit stiffness prediction tool. The method can therefore be used to replicate a case of practical interest, i.e. blades/dampers on a disk. In this case, the cyclic symmetry framework can be used to test different engine order excitations [36]: the left blade platform can be connected to the right one by  $K_I$  with a proper phase shift (i.e. inter-blade phase angle).

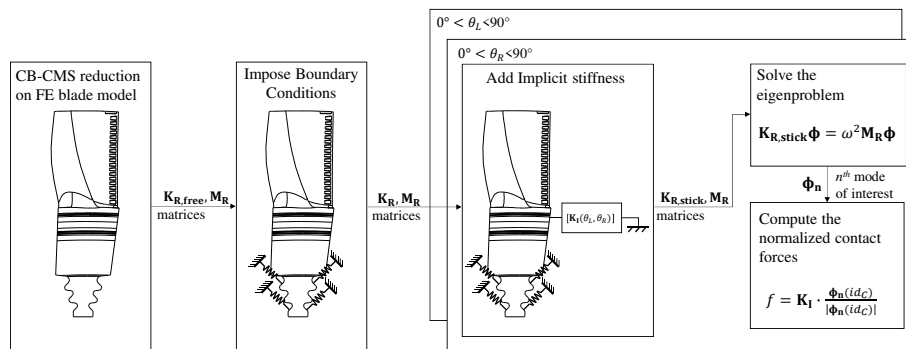


Figure 14: Graphical representation of the algorithm used to predict the normalized contact forces as a function of the blade platform angles.

## 6. Conclusions

This paper has presented a distinctive analysis procedure to investigate the dynamic behavior of the blade with under-platform dampers. The contact forces between the damper-blade contact interfaces were the prime focus of the study. Experimental data were obtained by using a test rig which offers the unique feature to measure the contact forces between the damper and the under-platform of the blade. In this test rig, two dampers were in contact with the respective platform of the blade. Knowledge of the contact forces combined with the forced-response of the blade has allowed a deeper

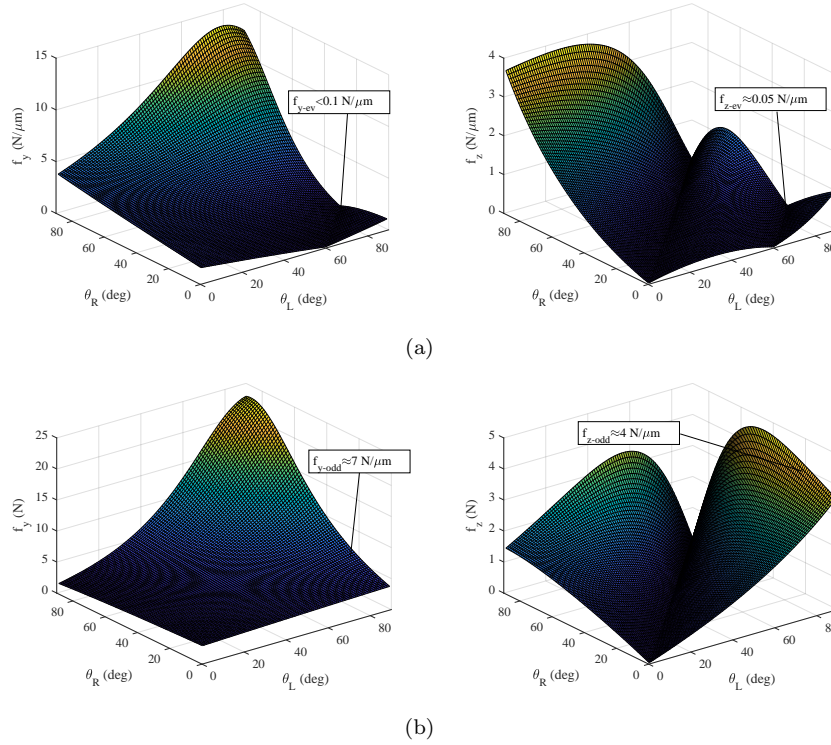


Figure 15:  $y$  and  $z$  components of the normalized contact force vector  $f$  when the damper is placed on the blade's (a) even and (b) odd side.

analysis of the dynamic behavior of the complete system. The blade was modeled with a commercial finite element code. In the next step, the mass and stiffness matrices of the blade were reduced, with a standard reduction order method, and extracted for further analysis to be performed with a in-house code. The reduced model was constrained to simulate the attachment between the blade and the slot machined in the turbine blade clamp adapter on the test rig. The attachment was simulated with contact springs assuming that no sliding occurs between the mating surfaces. During the experimental campaign contact forces at the blade-damper interface were measured

simultaneously with the forced-responses of the blade. These experimental evidence were used to verify whether the measured contact forces applied to the linear model of the blade yielded to a forced-response consistent with the measured response. The results of the comparison were excellent on one damper but unsatisfactory on the other one. To investigate this puzzling behavior, a sensitivity analysis based on the concept of equivalent implicit stiffness was performed on both dampers. This analysis showed that the contact forces evaluated on the damper that exhibited poor matching with the experimental results, were quite insensitive to the variation of damper geometry, namely the right and left contact angles. Moreover, these contact forces were very low and close to the measurement accuracy of the experimental system so that the determination of the value of these forces was an ill-conditioned problem. As a consequence, uncertainty in determining the contact forces value produces a large variation of the predicted force-response and then poor agreement with experimental results.

This work presents the validation of a contact models through experimental results under a different point of view. The main outcome is that when comparing the experimental results with a numerical simulation great attention must be paid to the source of experimental data. Some damper-underplatform configurations give contact forces that can be predicted with great uncertainty.

As underlined in the paper, in such conditions the computed forced-response of the blade is inaccurate, even if the measured contact forces are directly applied - during the simulation - to the contact nodes. The damper-underplatform geometry presented in this work is used in several friction

damping systems, therefore the results presented in this work warning for all the designers and researches involved in a validation process. The proposed methodology to predict the amplitude of the contact forces starting from the platform angles constitutes one of the main contributions of this paper, as  
 385 this methodology can be extended to the case of blades mounted on a disk in real working conditions.

### Appendix A. The implicit stiffness: derivation

With reference to Fig. 13a, let us consider the in-plane<sup>2</sup> equilibrium equations of a damper between a set of platforms with angles  $\theta_L$  and  $\theta_R$ .

$$\mathbf{M}_D \ddot{\mathbf{Q}}_D(t) = \mathbf{F}_{CD}(t) + \mathbf{F}_{ED} \quad (\text{A.1})$$

where  $\mathbf{Q}_D = (y_D, z_D, \beta_D)'$  is the vector of damper displacements,  $\mathbf{F}_{ED} = (0, CF, 0)'$  is the vector of external forces and  $\mathbf{F}_{CD}$  is the vector of contact forces transported at the damper center of mass. In case of full stick condition Eq. A.1 can be re-written as:

$$\mathbf{M}_D \ddot{\mathbf{Q}}_D(t) + \mathbf{K}_D \mathbf{Q}_D(t) = \mathbf{K}_P \mathbf{Q}_P(t) + \mathbf{F}_{ED} \quad (\text{A.2})$$

where  $\mathbf{Q}_P = (y_{LP}, z_{LP}, y_{RP}, z_{RP})'$  is the vector of platforms displacements (considered as an external information at this stage), and  $\mathbf{K}_D$  and  $\mathbf{K}_P$  are the contact stiffness matrices connected to damper and platforms respectively. The con-

---

<sup>2</sup>The following derivation holds for in-plane motion for simplicity. However, a 3D version can be easily implemented.

tact stiffness matrices can be expressed as:

$$\begin{aligned}\mathbf{K}_D &= \mathbf{T}'\mathbf{K}_{\text{local}}\mathbf{T} \\ \mathbf{K}_P &= \mathbf{T}'\mathbf{K}_{\text{local}}\mathbf{R}\end{aligned}\tag{A.3}$$

where matrix  $\mathbf{K}_{\text{local}}$  is diagonal and function of the contact stiffness values  $\mathbf{K}_{\text{local}} = \text{diag}(k_t, k_n, k_t, k_n)$ <sup>3</sup>. The reader will notice that the contact springs are oriented along the normal and tangential directions to each contact interface. For this reason, a local reference system has been defined for each interface (left and right).  $\mathbf{T}$  is a transformation matrix of forces and displacements from the global (damper center of mass) to the local (i.e. damper contact points) reference system and viceversa. Similarly  $\mathbf{R}$  is a rotation matrix from global to local reference system, used for the platforms DOFs. Both matrices are a function of the platform angles  $\theta_L$  and  $\theta_R$ . If variation of forces and displacements are considered, Eq. A.2 becomes:

$$\mathbf{K}_D\Delta\mathbf{Q}_D = \mathbf{K}_P\Delta\mathbf{Q}_P\tag{A.4}$$

where the inertial terms can be neglected as demonstrated in [35] and  $\Delta\mathbf{F}_{\text{ED}} = \mathbf{0}$  since the centrifugal force is a constant term. The damper displacement variation  $\Delta\mathbf{Q}_D$  is expressed as:

$$\Delta\mathbf{Q}_D = \mathbf{K}_D^{-1}\mathbf{K}_P\Delta\mathbf{Q}_P\tag{A.5}$$

Then the vector of contact forces in global coordinate system at the platform contact points can be expressed as:

$$\Delta\mathbf{F} = \mathbf{R}'\mathbf{K}_{\text{local}}(\mathbf{R} - \mathbf{T}\mathbf{K}_D^{-1}\mathbf{K}_P) \cdot \Delta\mathbf{Q}_P\tag{A.6}$$

---

<sup>3</sup>In case of 3D motion the matrix will become  $\mathbf{K}_{\text{local}} = \text{diag}(k_t, k_t, k_n, k_t, k_t, k_n)$ .

Where  $\Delta \mathbf{F} = (\Delta \mathbf{F}_{\text{LP},y}, \Delta \mathbf{F}_{\text{LP},z}, \Delta \mathbf{F}_{\text{RP},y}, \Delta \mathbf{F}_{\text{RP},z})'$  is the vector of contact forces on the two blade platforms. It is then possible to write:

$$\Delta \mathbf{F} = \mathbf{K}_{\mathbf{I}}^* \Delta \mathbf{Q}_{\mathbf{P}} \quad (\text{A.7})$$

where  $\mathbf{K}_{\mathbf{I}}^*$  has the following structure:

$$\mathbf{K}_{\mathbf{I}}^* = \begin{bmatrix} \mathbf{K}_{\mathbf{I}} & -\mathbf{K}_{\mathbf{I}} \\ -\mathbf{K}_{\mathbf{I}} & \mathbf{K}_{\mathbf{I}} \end{bmatrix} = \begin{bmatrix} k_{yy} & k_{yz} & -k_{yy} & -k_{yz} \\ k_{yz} & k_{zz} & -k_{yz} & -k_{zz} \\ -k_{yy} & -k_{yz} & k_{yy} & k_{yz} \\ -k_{yz} & -k_{zz} & k_{yz} & k_{zz} \end{bmatrix} \quad (\text{A.8})$$

The matrix  $\mathbf{K}_{\mathbf{I}}$  is here termed implicit stiffness matrix and can be used to  
 390 link a blade to a neighboring structure, be it an adjacent blade (real working  
 conditions) or a ground platform (test rig condition).

## References

- [1] J. H. Griffin, Friction damping of resonant stresses in gas turbine engine  
 airfoils, J. Eng. Power 102 (2) (1980) 329–333 (1980). doi:10.1115/1.3230256.  
 395
- [2] W. Sextro, K. Popp, I. Wolter, Improved reliability of bladed disks  
 due to friction dampers, in: ASME Turbo Expo: Power for Land,  
 Sea, and Air, Vol. 4: Manufacturing Materials and Metallurgy; Ceram-  
 ics; Structures and Dynamics; Controls, Diagnostics and Instrumenta-  
 400 tion; Education, Orlando, Florida, USA, 1997, p. V004T14A035 (1997).  
 doi:10.1115/97-GT-189.

- 405 [3] B. D. Yang, C. H. Menq, Characterization of contact kinematics and application to the design of wedge dampers in turbomachinery blading: part 1—stick-slip contact kinematics, *J. Eng. Gas Turbines Power* 120 (2) (1998) 410–417 (apr 1998). doi:10.1115/1.2818138.
- [4] B. D. Yang, C. H. Menq, Characterization of contact kinematics and application to the design of wedge dampers in turbomachinery blading: part 2—prediction of forced response and experimental verification, *J. Eng. Gas Turbines Power* 120 (2) (1998) 418–423 (apr 1998). doi:10.1115/1.2818139.  
410
- [5] G. Csaba, Modelling of a microslip friction damper subjected to translation and rotation, in: *ASME 1999 International Gas Turbine and Aero-engine Congress and Exhibition*, American Society of Mechanical Engineers, 1999, pp. V004T03A012–V004T03A012 (1999).
- 415 [6] K. Y. Sanliturk, D. J. Ewins, A. B. Stanbridge, Underplatform dampers for turbine blades: theoretical modelling, analysis and comparison with experimental data, in: *ASME 1999 international gas turbine and aero-engine congress and exhibition*, American Society of Mechanical Engineers, 1999, pp. V004T03A037–V004T03A037 (1999).
- 420 [7] L. Panning, W. Sextro, K. Popp, Optimization of interblade friction damper design, in: *ASME Turbo Expo: Power for Land, Sea, and Air*, Vol. 4: Manufacturing Materials and Metallurgy; Ceramics; Structures and Dynamics; Controls, Diagnostics and Instrumentation; Education, Munich, Germany, 2000, p. V004T03A068 (2000).  
425 doi:10.1115/2000-GT-0541.

- [8] E. P. Petrov, D. J. Ewins, Analytical formulation of friction interface elements of nonlinear multi-harmonic vibrations of bladed discs, in: ASME (Ed.), Turbo Expo: Power for Land, Sea, and Air, Vol. 4: Turbo Expo 2002, Parts A and B, Amsterdam, 2002, pp. 899–908 (2002).  
430 doi:10.1115/GT2002-30325.
- [9] S. Zucca, D. Botto, M. M. Gola, Range of variability in the dynamics of semi-cylindrical friction dampers for turbine blades, in: ASME Turbo Expo 2008: Power for Land, Sea, and Air, American Society of Mechanical Engineers, ASME, 2008, pp. 519–529 (2008). doi:  
435 10.1115/GT2008-51058.
- [10] L. Pesaresi, L. Salles, A. Jones, J. Green, C. Schwingshackl, Modelling the nonlinear behaviour of an underplatform damper test rig for turbine applications, Mech. Syst. Sig. Process. 85 (2017) 662–679 (2017). doi:  
10.1016/j.ymssp.2016.09.007.
- 440 [11] C. W. Schwingshackl, E. P. Petrov, D. J. Ewins, Effects of contact interface parameters on vibration of turbine bladed disks with underplatform dampers, J. Eng. Gas Turbines Power 134 (3) (2012) 032507 (2012).  
doi:10.1115/1.4004721.
- [12] C. Gastaldi, Modeling Friction for Turbomachinery Applications: Tuning Techniques and Adequacy Assessment of Heuristic Contact Models,  
445 InTech, 2018 (2018). doi:10.5772/intechopen.72676.
- [13] M. Umer, D. Botto, Measurement of contact parameters on under-

platform dampers coupled with blade dynamics, *Int. J. Mech. Sci.* (2019). doi:10.1016/j.ijmecsci.2019.06.010.

- 450 [14] I. A. Sever, E. P. Petrov, D. J. Ewins, Experimental and numerical investigation of rotating bladed disk forced response using underplatform friction dampers, *ASME J. Eng. Gas Turbines Power* 130 (4) (2008) 042503–11 (2008). doi:10.1115/1.2903845.
- [15] T. Berruti, A test rig for the investigation of the dynamic response of a  
455 bladed disk with underplatform dampers, *Mech. Res. Commun.* 37 (6) (2010) 581–583 (2010). doi:10.1016/j.mechrescom.2010.07.008.
- [16] A. Bessone, F. Toso, T. Berruti, Investigation on the dynamic response of blades with asymmetric under platform dampers, in: *ASME Turbo Expo: Power for Land, Sea, and Air, Vol. 7B: Structures and Dynamics*, Montreal, Quebec, Canada, 2015, p. V07BT33A003 (June 15–9 2015).  
460 doi:10.1115/GT2015-42597.
- [17] C. W. Schwingshackl, E. P. Petrov, D. J. Ewins, Validation of test rig measurements and prediction tools for friction interface modelling, in: *ASME Turbo Expo: Power for Land, Sea, and Air, Vol. 6, 2010* (2010).  
465 doi:10.1115/GT2010-23274.
- [18] D. Botto, M. Lavella, M. M. Gola, Measurement of contact parameters of flat on flat contact surfaces at high temperature, in: *Volume 7: Structures and Dynamics, Parts A and B*, ASME, 2012 (jun 2012). doi:10.1115/GT2012-69677.

- 470 [19] D. Botto, M. Lavella, High temperature tribological study of cobalt-based coatings reinforced with different percentages of alumina, *Wear* 318 (1-2) (2014) 89–97 (oct 2014). doi:10.1016/j.wear.2014.06.024.
- [20] M. Lavella, D. Botto, M. M. Gola, Design of a high-precision, flat-on-flat fretting test apparatus with high temperature capability, *Wear* 302  
475 (2013) 1073–1081 (2013). doi:10.1016/j.wear.2013.01.066.
- [21] M. M. Gola, M. Braga dos Santos, T. Liu, Design of a new test rig to evaluate underplatform damper performance, in: *ASME 2010 10th Biennial Conference on Engineering Systems Design and Analysis*, Vol. 5, 2010, pp. 85–95 (2010). doi:10.1115/ESDA2010-24268.
- 480 [22] C. Gastaldi, M. M. Gola, A random sampling strategy for tuning contact parameters of underplatform dampers, in: *Volume 7B: Structures and Dynamics*, ASME International, 2015 (jun 2015). doi:10.1115/GT2015-42834.
- [23] C. Gastaldi, M. M. Gola, Pre-optimization of asymmetrical underplatform dampers, *J. Eng. Gas Turbines Power* 139 (1) (2016) 1229 (aug  
485 2016). doi:10.1115/1.4034191.
- [24] D. Botto, C. Gastadi, M. M. Gola, M. Umer, An experimental investigation of the dynamics of a blade with two under-platform dampers, *J. Eng. Gas Turbines Power* 140 (3) (2017) 032504 (oct 2017). doi:  
490 10.1115/1.4037865.
- [25] D. Botto, M. Umer, A novel test rig to investigate under-platform

damper dynamics, *Mech. Syst. Sig. Process.* 100 (2018) 344–359 (feb 2018). doi:10.1016/j.ymssp.2017.07.046.

[26] C. Gastaldi, T. M. Berruti, M. M. Gola, A novel test rig for friction parameters measurement on underplatform dampers, *Int. J. Solids Struct.* (aug 2019). doi:10.1016/j.ijsolstr.2019.08.030.

[27] R. Craig, M. Bampton, Coupling of substructures for dynamic analyses, *AIAA journal* 6 (7) (1968) 1313–1319 (jul 1968). doi:10.2514/3.4741.

[28] W. C. Hurty, Dynamic analysis of structural systems using component modes, *AIAA journal* 3 (4) (1965) 678–685 (1965).

[29] T. M. Cameron, J. H. Griffin, An alternating frequency/time domain method for calculating the steady-state response of nonlinear dynamic systems, *J. Appl. Mech.* 56 (1) (1989) 149–154 (1989).

[30] A. Cardona, T. Coune, A. Lerusse, M. Geradin, A multiharmonic method for non-linear vibration analysis, *Int. J. Numer. Methods Eng.* 37 (9) (1994) 1593–1608 (1994).

[31] C. M. Firrone, S. Zucca, M. M. Gola, The effect of underplatform dampers on the forced response of bladed disks by a coupled static/dynamic harmonic balance method, *Int. J. Non Linear Mech.* 46 (2) (2011) 363–375 (2011). doi:10.1016/j.ijnonlinmec.2010.10.001.

[32] M. Krack, L. Salles, F. Thouverez, Vibration prediction of bladed disks coupled by friction joints, *Arch. Comput. Methods Eng.* (jul 2016). doi:10.1007/s11831-016-9183-2.

- 515 [33] C. Gastaldi, M. M. Gola, Criteria for best performance of pre-optimized solid dampers, *J. Eng. Gas Turbines Power* 141 (4) (2018) 042502 (nov 2018). doi:10.1115/1.4040820.
- [34] M. Umer, C. Gastadi, D. Botto, The effect of friction damping on the dynamic response of vibrating structures: An insight into model validation, in: *Proceedings of ISMA 2018 - International Conference on Noise and Vibration Engineering and USD 2018 - International Conference on Uncertainty in Structural Dynamics*, 2018, pp. 1021–1035 (2018).  
520
- [35] C. Gastaldi, *Vibration control and mitigation in turbomachinery*, Ph.D. thesis, Politecnico di Torino Italy (2017). doi:10.6092/polito/porto/2677053.  
525
- [36] C. Gastaldi, T. M. Berruti, M. M. Gola, Best practices for underplatform damper designers, *Proceedings of the Institution of Mechanical Engineers, Part C: Journal of Mechanical Engineering Science* 232 (7) (2018) 1221–1235 (feb 2018). doi:10.1177/0954406217753654.